Phenotypic Screening Identifies Protein Synthesis Inhibitors as H-Ras-Nanocluster-Increasing Tumor Growth Inducers

ARTICLE *in* BIOCHEMISTRY · NOVEMBER 2015

Impact Factor: 3.02 · DOI: 10.1021/acs.biochem.5b00724

9 AUTHORS, INCLUDING:

Arafath Kaja Najumudeen

Turku Centre for Biotechnology

5 PUBLICATIONS **14** CITATIONS

SEE PROFILE

Yong Zhou

University of Texas Health Science Center at H…

28 PUBLICATIONS **467** CITATIONS

SEE PROFILE

Adyary Fallarero

Faculty of Pharmacy, University of Helsinki, Fi…

56 PUBLICATIONS **653** CITATIONS

SEE PROFILE

Daniel Abankwa

Åbo Akademi University

42 PUBLICATIONS **1,296** CITATIONS

SEE PROFILE

BIOCHEMISTRY
including biophysical chemistry & molecular biology

Article

pubs.acs.org/biochemistry

Phenotypic Screening Identifies Protein Synthesis Inhibitors as H-Ras-Nanocluster-Increasing Tumor Growth Inducers

Arafath K. Najumudeen,[†] Itziar M. D. Posada,[†] Benoit Lectez,[†] Yong Zhou,[‡] Sebastian K.-J. Landor,[†,§] Adyary Fallarero,[∥] Pia Vuorela,[∥] John Hancock,[‡] and Daniel Abankwa*[,†]

[†]Turku Centre for Biotechnology, Åbo Akademi University, Tykistökatu 6B, 20520 Turku, Finland

[‡]University of Texas Health Science Center at Houston, Medical School, Houston, Texas 77030, United States

[§]Department of Cell and Molecular Biology (CMB), Karolinska Institutet, SE-171 77 Stockholm, Sweden

[∥]Division of Pharmaceutical Biosciences, Faculty of Pharmacy, University of Helsinki, FI-00014 Helsinki, Finland

Supporting Information

ABSTRACT: Ras isoforms H-, N-, and K-ras are each mutated in specific cancer types at varying frequencies and have different activities in cell fate control. On the plasma membrane, Ras proteins are laterally segregated into isoform-specific nanoscale signaling hubs, termed nanoclusters. As Ras nanoclusters are required for Ras signaling, chemical modulators of nanoclusters represent ideal candidates for the specific modulation of Ras activity in cancer drug development. We therefore conducted a chemical screen with commercial and in-house natural product libraries using a cell-based H-ras-nanoclustering FRET assay. Next to established Ras inhibitors, such as a statin and farnesyl-transferase inhibitor, we surprisingly identified five protein synthesis inhibitors as positive regulators. Using commonly employed cycloheximide as a representative compound, we show that protein synthesis inhibition increased nanoclustering and effector recruitment specifically of active H-ras but not of K-ras. Consistent with these data, cycloheximide treatment activated both Erk and Akt kinases and specifically promoted H-rasG12V-induced, but not K-rasG12V-induced, PC12 cell differentiation. Intriguingly, cycloheximide increased the number of mammospheres, which are enriched for cancer stem cells. Depletion of H-ras in combination with cycloheximide significantly reduced mammosphere formation, suggesting an exquisite synthetic lethality. The potential of cycloheximide to promote tumor cell growth was also reflected in its ability to increase breast cancer cell tumors grown *in ovo*. These results illustrate the possibility of identifying Ras-isoform-specific modulators using nanocluster-directed screening. They also suggest an unexpected feedback from protein synthesis inhibition to Ras signaling, which might present a vulnerability in certain tumor cell types.

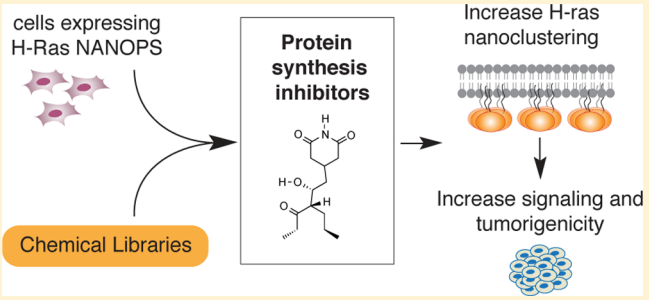

Targeting oncogenic proteins with small molecules has been a successful therapeutic strategy with considerable clinical responses.[1] However, relapse after therapy occurs frequently and is attributed to the evolution of resistant clones.[2] The cancer stem cell model provides the background for the hierarchical organization of cancer cell clones within tumors. Cancer stem cells (CSCs) are endowed with a self-renewal potential similar to that of normal stem cells, which enables them to seed tumors. Importantly, CSCs give rise to differentiated progeny that constitutes the bulk tumor mass, which is responsive to standard chemotherapeutics, whereas CSCs are not.[3] This has led to the concept of treating cancer (stem) cells with small molecules to selectively drive their differentiation by selective activation and modulation of signaling pathways.[4]

On the molecular level, oncogene addiction is the leading concept for targeted therapy development. However, some of the most frequently activated oncogenes in cancer are still associated with poor response to standard therapies.[5,6] Ras family proteins, which are among the most notorious human oncogenes, are a classic example with an undruggable profile. This is ascribed to their structural and biochemical properties as well as to the apparent promiscuity of their signaling activity.[7]

Indeed, all cancer-associated Ras isoforms promote cell growth and survival *in vitro* by activating in particular the Raf−Erk and PI3K−Akt signaling pathways.[8,9] However, Ras isoforms not only have very different mutation frequencies and cancer profiles[10] but also different roles during development.[11,12] Recent data suggest that H-ras drives differentiation, N-ras is apparently neutral, and K-ras4B (hereafter, K-ras) stimulates self-renewal of stem cells.[13] Considering that the orchestration of these developmental processes is out of control in tumors, as exemplified in teratomas, the specific regulation of

Received: June 28, 2015
Revised: October 16, 2015

DOI: 10.1021/acs.biochem.5b00724
Biochemistry XXXX, XXX, XXX−XXX

each Ras isoform needs to be understood for successful cancer treatment. In addition, Costello syndrome is a developmental disease caused by germline mutations of H-ras.[14] Currently, no treatment for Costello syndrome exists.

The application of advanced quantitative imaging techniques, such as electron microscopy and fluorescence microscopic methods,[15−17] revealed that Ras isoforms H-, N-, and K-ras are laterally segregated on the plasma membrane into distinct, nanoscale signaling hubs called nanoclusters.[18] Nanocluster contain 6−8 Ras proteins, which become immobilized in nanoclusters upon their activation.[15,19] Nanoclusters can be stabilized by scaffolding proteins, such as galectin-1 (Gal-1), which specifically increases H-ras nanoclustering and potentiates its Raf and Erk signaling output.[9,20] Given that nanoclusters are essential for Ras signaling,[21] they represent ideal targets for the isoform-specific modulation of Ras activity.

We have recently described the identification of macrotetrolides as negative modulators of H-ras nanoclusters.[22] Here, we describe the discovery of the first positive chemical modulators of Ras nanocluster. We built on our well-established FRET-based chemical screening approach.[22−25] Surprisingly, we found that protein synthesis inhibitors, such as cycloheximide, specifically enhance H-ras nanoclustering, signaling, and tumor growth. This study illustrates how Ras-nanocluster-directed screening could yield Ras-isoform-specific chemical modulators that could find applications as research tools in cancer drug development.

EXPERIMENTAL PROCEDURES

Cell Culture and DNA Constructs. Baby hamster kidney (BHK) 21, wild-type and Du-315-6 (H-ras$^{-/-}$, N-ras$^{-/-}$)[26] mouse embryonic fibroblast (MEF), and human embryonic kidney 293-EBNA (HEK)[27] cells were cultured in Dulbecco's modified Eagle's medium (DMEM, Invitrogen) supplemented with 10% fetal bovine serum, 1% L-glutamine, 100 U/mL of penicillin, and 100 μg/mL streptomycin. Rat adrenal pheochromocytoma (PC12) cells were cultured on plates coated with 50 μg/mL of rat tail collagen I (Gibco) in Roswell Park Memorial Institute (RPMI)-1640 medium (Invitrogen) supplemented with 10% horse serum, 5% FBS, 1% L-glutamine, 100 U/mL penicillin, and 100 μg/mL streptomycin. MDA-MB-231 breast cancer cells were cultured in RPMI-1640 medium (Invitrogen) supplemented with 10% fetal bovine serum and 1% L-glutamine. All cells were incubated at 37 °C under 5% CO_2. Transfections were performed with jetPRIME (Polyplus transfection) according to the manufacturer's instructions in a 6-well plate, unless stated otherwise. Plasmids encoding the C-terminal hypervariable region of human H-ras (H-ras-NANOPS; previously referred to as CTH) genetically fused to monomeric cyan fluorescent protein (mCFP) and monomeric citrine (mCitrine) have been described previously.[22] Plasmids pmGFP-H-rasG12V, pmGFP-K-ras4BG12V, and mRFP-RBD of C-Raf were described previously.[28,29] Plasmids used for either overexpression (pcDNA3-Gal-1) or knockdown (pcDNA3-asGal-1) of untagged galectin-1 have been previously described by others.[30] Plasmids pmCherry-H-rasG12V and pmCherry-K-rasG12V constructs were generated by replacing pmGFP from pmGFP-H-rasG12V and pmGFP-K-rasG12V with pmCherry from pmCherry-C1 vector (Clontech Laboratories Inc., CA, USA) using NheI and BsrGI restriction sites. siRNA directed against H-ras has been previously described by others.[31]

Chemical Screening with H-Ras-NANOPS, Data Acquisition, and Analysis. For chemical screening, 659 compounds from two different sources were used: a commercially available Enzo Screen-Well Natural Product Library (Enzo Life Sciences Inc., USA), consisting of 502 naturally derived compounds, and an in-house diverse natural collection of 157 compounds.[32,33] The in-house collection contained diverse natural compounds obtained from different commercial suppliers. The list of all tested compounds is included in Supporting Information Table 1. Chemical library screens were performed with BHK cells seeded in 6-well plates and transfected with H-Ras-NANOPS using jetPRIME. Eighteen hours after transfection, cells were transferred to 96-well plates at 50 000 cells/well in 250 μL of cell culture media. After the cells attached (5−7 h), they were treated for an additional 24 h with 5 μL of compounds (10 μM final concentration) from the chemical libraries. The final DMSO concentration was 2% v/v. Afterward, cells were detached with 75 μL of 5 mM EDTA in PBS and fixed for 15 min by adding 75 μL of 4% paraformaldehyde (PFA) in PBS. The samples were then stored at 4 °C until analysis. The screen was performed with at least three independent biological repeats. Each 96-well plate was designed to have an internal positive control (compactin at 5 μM). Hits satisfying the selection criterion of 15% change in E_{max} were selected for further analysis. Autofluorescence (if any) of the primary hits was measured in the fluorescence range from 405 to 600 nm with excitation at both 405 nm (donor excitation in cytometer screen) and 488 nm (acceptor excitation in cytometer screen), and hits with high autofluorescence were eliminated from further analysis. Cycloheximide (cat. no. 0970, Fischer Scientific) and other hits were repurchased from Fischer Scientific or Sigma-Aldrich, and validations were performed in BHK and HEK cells. Cells were analyzed in a FACS LSRII (BD Biosciences) equipped with a high-throughput sampler (HTS) unit, using the filters for donor-channel (405 nm excitation, 450/50 nm emission filter), acceptor-channel (488 nm excitation, 530/30 nm emission filter), and FRET-channel (405 nm excitation, 585/42 nm emission filter). The flow cytometer data were analyzed with a custom-written procedure in IgorPro.[24,34] In brief, doublet discrimination was implemented to measure signals of single cells. For normalized acceptor level calibration (cA), FITC beads (Bangs Laboratories) with a defined size and fluorescein content were used. A mCFP−mCit fusion protein was used to calibrate for the FRET efficiency and donor−acceptor ratio. Only cells with a donor mole fraction $x_D = 0.5 \pm 0.1$ were analyzed. The E_{max} value was determined as described.[24]

Immunoelectron Microscopic Analysis of Ras Nanoclustering. Immunoelectron microscopy spatial mapping was performed as described previously.[16,35] Apical plasma membrane sheets were prepared, fixed with 4% PFA/PBS and 0.1% glutaraldehyde, and labeled with 4.5 nm (diameter) gold nanoparticles coupled to anti-GFP antibody. Digital images of the immuno gold-labeled plasma membrane sheets were taken at 100 000× magnification in an electron microscope (Jeol JEM-1400). Intact 1 mm^2 areas of the plasma membrane sheet were identified using ImageJ, and the (x, y) coordinates of the gold particles were determined as described. A minimum of 15 plasma membrane sheets were imaged and analyzed for each condition. A bootstrap test constructed as previously described was then used to evaluate the statistical significance of differences between replicated point patterns.[15]

DOI: 10.1021/acs.biochem.5b00724
Biochemistry XXXX, XXX, XXX−XXX

Fluorescence Lifetime Imaging Microscopy (FLIM)-FRET. BHK cells were seeded on a 6-well plate with glass coverslips, and transfection was done after 24 h using jetPRIME (Polyplus) transfection reagent with the following plasmids: pmGFP-H-rasG12V or pmGFP-K-rasG12V alone or together with pmCherry-H-rasG12V or pmCherry-K-rasG12V, respectively (pmGFP/pmCherry plasmids at a 1:3 ratio, 2 μg total plasmid), and pmGFP-H-rasG12V or pmGFP-K-rasG12V cotransfected with pmCherry-C-Raf-RBD (1:3 ratio). Twenty-four hours after transfection, cells were treated for 24 h with either control (DMSO 0.05% (v/v)) or 0.18 or 10 μM CHX and incubated for an additional 24 h. DMSO concentration in the final samples was less than 0.05% (v/v). Cells were fixed in 4% PFA/PBS for 20 min and then washed in PBS, and coverslips with cells were then mounted with Mowiol 4-88 (Sigma-Aldrich, cat. no. 81381) on microscope slides. FLIM-FRET measurements were done using a lifetime fluorescence imaging attachment (Lambert Instruments, Groningen, Netherlands) on an inverted microscope (Zeiss AXIO Ovserver.D1, Jena, Germany). Samples were excited with sinusoidally modulated (40 MHz) epi-illumination at 3 W and 470 nm using a temperature-stabilized multi-LED system (Lambert Instruments). Cells were imaged with a 63×,1.4 NA oil objective using an appropriate GFP filter set (excitation, bandpass 470/40; beam splitter, FT 495; emission, bandpass 535/50). The phase and modulation fluorescence lifetimes were determined per pixel from images acquired at 12 phase settings using the manufacturer's software. Fluorescein (10 μM in Tris buffer, pH 9.0) was used as a lifetime reference standard (lifetime, 4.0 ns). The percentage of the apparent FRET efficiency (E_{app}) was calculated using the measured lifetimes of each donor−acceptor pair (τ_{DA}) and the average lifetime of the donor-only (τ_D) samples. The formula employed was $E_{app} = (1 - \tau_{DA}/\tau_D) \times 100\%$.

Fluorescence Recovery after Photobleaching (FRAP). FRAP was used to monitor diffusion properties of mGFP tagged H-rasG12V in BHK cells treated for 24 h with either control (DMSO 0.05% (v/v)), Gal-1 overexpression, Gal-1 depletion, or CHX treatment. Treatments were performed 24 h after transfection. DMSO concentrations in the final samples were 0.05% (v/v). Cells were kept in Ringers buffer (10 mM HEPES, 10 mM glucose, 2 mM $NaH_2PO_4 \cdot H_2O$, 1 mM $MgCl_2 \cdot 6H_2O$, 2 mM $CaCl_2$, 5 mM KCl, 155 mM NaCl, pH 7.2) at 37 °C. All data were acquired on a Zeiss LSM 780 microscope (Carl Zeiss AG, Jena, Germany) using the Time Series and Bleaching functions included by the manufacturer in their Zen software. Cells were imaged using confocal microscopy (excitation, 488 nm; detection, 493−575 nm) with unidirectional scanning and a pixel dwell time of 0.79 μs. Scanning was done at a 512 × 512 resolution and with a 15× zoom (pixel size, 0.0176 μm). Under these conditions, we obtained a time between frames of 0.243 s. The first 10 frames were taken with only 2% of the argon laser intensity (laser nominal power is 35 mW) and were used as a reference for normalization. Bleaching was performed on a circular region of interest of 2 μm diameter using the full laser power until the fluorescence signal in the region was reduced to 40% of the initial intensity. To monitor the recovery, an additional 40−60 frames were taken with 2% of the laser intensity. Fluorescence signals were quantified using the FRAP View tool provided in our Zeiss LSM 780 microscope, and values were exported as a text file (.txt) for further analysis. The apparent characteristic half time of recovery and the immobile fraction were determined using curve fitting analysis in IGOR Pro 6 (WaveMetrics, Tigard, OR, USA) according to the following formula by Feder et al.[36]

$$F(t) = \frac{F_0 + F_\infty\left(\frac{t}{t_{1/2}}\right)}{1 + \left(\frac{t}{t_{1/2}}\right)}$$

In this equation, $F(t)$ represents the normalized fluorescence intensity, t is the time, F_∞ is the normalized intensity after an infinite time, $t_{1/2}$ is the half time of recovery, and F_0 is the fluorescence intensity at $t = 0$, immediately after bleaching. Immobile fractions Q were calculated using $Q = (1 - F_\infty)/(1 - F_0)$. For each sample, approximately 30 cells were measured from three independent experiments.

Western Blot Analysis. BHK, wild-type MEF, and Du-315-6 Rasless MEF (H-ras$^{-/-}$, N-ras$^{-/-}$) cells were cultured in Dulbecco's modified Eagle's medium (DMEM) supplemented with 10% FBS and L-glutamine. For H-ras rescue experiments, Du-315-6 cells were transfected with GFP-wt-H-ras using Lipofectamine 3000 (Thermo-Fischer Scientific) according to the manufacturer's instructions. Cells were treated for 24 h with either control (DMSO 0.05% (v/v)) or 0.18 or 10 μM CHX and then harvested using a buffer containing 50 mM dithiothreitol, 2% SDS, 10% glycerol, 0.1% bromophenol blue, and 10 mM Tris-HCl, pH 6.8. Proteins were first separated using SDS-PAGE (10%) and then electroblotted on a nitrocellulose membrane (GE Healthcare). Membranes were immunolabeled using primary antibodies against Erk1/2 (Cell Signaling Technology, cat. no. 9102), ppErk1/2 (T202/Y204; Cell Signaling Technology, cat. no. 9101), Akt (Cell Signaling Technology, cat. no. 9272), and pAkt (T308; R&D Systems, cat. no. 658320). β-Actin antibody (Sigma-Aldrich, cat. no. A1978) was used as a loading control. Horseradish peroxidase-conjugated goat anti-rabbit and chicken anti-mouse IgG antibodies (Santa Cruz Biotechnology, cat. nos. sc-2004 and sc-2954) were used as secondary antibodies. Protein bands were detected with enhanced chemiluminiscence (Clarity Western ECL blotting, Bio-Rad), and quantification of the signal intensities was performed using ImageLab software (Bio-Rad).

PC12 Cell Differentiation Assay. PC12 cells were plated in a 8-well Lab-Tek chambered coverglass (Nunc Thermo Fischer Scientific) coated with 0.1% rat tail collagen I in 30% ethanol. After 24 h, cells were transfected with GFP-H-rasG12V or GFP-K-rasG12V using Lipofectamine 3000 (Thermo-Fischer Scientific). Forty-eight hours after transfection, cells were treated for 3 days with either DMSO (control) or 0.18 μM CHX. GFP-expressing cells were imaged using an EVOS FL imaging system, and cells were scored for extension of neurites longer than 1.5 times the size of the cell soma. For each experimental condition, at least 100 GFP positive cells from four independent biological repeats were analyzed.

Mammosphere Assay. MDA-MB-231 cells were cultured in 48-well suspension culture plates (Cellstar, Greiner Bio-One) at an initial density of 2000 cells/well in serum-free RPMI supplemented with 1× B27 (Gibco/Thermo Fisher), 25 ng/mL EGF (Sigma), and 25 ng/mL FGF (Sigma). After 6 days in culture, cells were treated for additional 3 days with CHX at 10 μM. For RNAi experiments, cells were first seeded in 6-well plates and transfected with either 125 nM scrambled siRNA or siRNA targeting H-ras,[31] and 24 h later they were transferred to 48-well suspension culture plates and treated as

DOI: 10.1021/acs.biochem.5b00724
Biochemistry XXXX, XXX, XXX−XXX

mentioned above. The mammospheres were analyzed in an Evos FL microscope (Thermo Fisher Scientific), and spheres with a minimum size of 50 μM were counted.

***In Ovo* Tumor Growth.** Fertilized chicken eggs were placed in an egg incubator under rotation in 37 °C and 60% humidity on day 1 of embryonic development. On day 3, the eggs were turned, taken off rotation, and punctured to create a small hole, which was then covered with adhesive tape. On day 8, the holes were expanded, and a small plastic ring (5−6 mm in diameter) was placed on top of the chorioallantoic membrane (CAM). Subsequently, 2×10^6 MDA-MB-231 cells were suspended in a 1:1 mixture of PBS and matrigel (BD Biosciences) for a total volume of 30 μL/egg and transplanted inside the plastic ring on the CAM, whereafter the eggs were sealed with parafilm. Tumors were treated daily either with control (DMSO 0.05% (v/v) in PBS) or 10 μM CHX in PBS. On day 13, the tumors were excised and fixed in 3% PFA overnight in +4 °C (or 1 h at room temperature), after which the tumors were dehydrated with an ethanol series of 50, 70, 70% for 1 h each at room temperature and finally in 70% ethanol at +4 °C overnight. The tumors were weighed in 70% ethanol using an analytical laboratory scale.

Statistical Analysis. Statistical differences in FLIM-FRET, FRAP, PC12 differentiation, and mammosphere experiments were determined using an analysis of variance (ANOVA) complemented by Tukey's honest significance difference test (Tukey's HSD) performed in GraphPad Prism. Statistical significance levels are annotated as ns, not significant; *, $p < 0.05$; **, $p < 0.01$; ***, $p < 0.001$; and ****, $p < 0.0001$. Statistical differences in western blotting and *in ovo* tumor growth were determined using Student's t test performed in GraphPad Prism. Statistical significance levels are annotated as *, $p < 0.05$; **, $p < 0.01$; and ***, $p < 0.001$.

RESULTS AND DISCUSSION

Compound Screening with an H-Ras-Specific FRET Biosensor Identifies Protein Synthesis Inhibitors as Positive Modulators of H-Ras Nanoclustering. Different Ras isoforms are laterally segregated into distinct nanoclusters on the plasma membrane, and these nanoclusters are essential for Ras signaling.[18] The fact that nanoclusters are isoform-specific presents the opportunity to pharmacologically modulate the activity of only one specific Ras isoform.

In order to identify novel chemical modulators of H-ras, we employed our recently reported cellular H-ras-NANOPS (NANOclustering and Prenylation Sensor) FRET assay. While FRET in this assay emerges from the nanoclustered biosensors, it detects changes not only in nanoclustering but also of any other event upstream of it, including, but not limited to, mislocalization from the plasma membrane and blockage of lipid modifications. BHK cells expressing the H-Ras FRET biosensor were screened with 659 small molecules from the commercially available Enzo Screen-Well natural product library supplemented by a chemically diverse in-house natural compound collection[32,33] in a 96-well format at an average concentration of 10 μM (Figure 1a). A Z'-factor of 0.6 and coefficient of variation (% CV) of 5% qualified our assay as excellent, allowing us to implement a hit selection criterion of ≥15% change in FRET signal from the average. Thus, we identified 38 primary hits, from which we excluded 14 due to autofluorescence (final 3.6% hit rate) (Figure 1b and Supporting Information Table 2). We then cross-validated these primary hits in a human cell line (HEK), leaving 12 confirmed compounds for further evaluation (Figure 1c). Results obtained from both cell lines showed a good correlation (Supporting Information Figure 1a), supporting the reproducibility of our assay. Validated hits included six compounds (negative deviators) that reduced the FRET signal and six compounds (positive deviators) that surprisingly increased the FRET signal of H-ras-NANOPS in at least one of the cell lines (Figure 1c and Supporting Information Table 3).

The negative deviators (Supporting Information Table 3) included diverse compound classes such as the well-established HMG-CoA inhibitor mevastatin[37] and the farnesyl transferase (FTase) inhibitor dihydrotanshinone.[38] The latter two compounds both block the farnesylation and therefore the membrane anchorage of the biosensor, thus leading to a decrease in the FRET signal.[22] The identification of these inhibitors corroborated the potential of our assay to identify pharmacologically interesting compounds that can affect Ras nano- and microscopic membrane organization.

However, we were more intrigued by the fact that five out of six positive deviators were structurally highly divergent protein synthesis inhibitors (PSI) (Supporting Information Table 3), including the frequently employed cycloheximide (CHX). Many of these PSI are routinely used in cell biology, and their activity with respect to cell signaling and differentiation has been described before.[39−41] However, a specific effect of CHX and other PSIs specifically on Ras nanoclustering is unknown.

Cycloheximide Increases H-Ras Nanoclustering. Only one nanocluster scaffold, the small β-galactoside binding protein galectin-1 (Gal-1), is known to positively and specifically regulate nanoclustering of active H-ras.[20,30,42] We recently found evidence that this protein may play a significant role in defining the stemness vs differentiated state of cells (A.K. Najumudeen and D. Abankwa, unpublished results). Given the suggested role of H-ras as a regulator of stem cell differentiation,[13] compounds that can positively modulate H-ras nanoclustering and signaling could be highly relevant in cellular reprogramming technology or cancer (differentiation) therapy.[4,43] Moreover, recent data suggest that small molecule Raf inhibitors lead to paradoxical Raf activation because they specifically increase K-ras and N-ras nanoclustering.[44,45] Hence, we decided to investigate the effect of protein synthesis inhibitors on Ras nanoclustering, using cycloheximide as the representative compound.

We first examined the nanoscale distribution of constitutively active H-rasG12V and its wild-type (wt) counterpart on the inside of the plasma membrane of BHK cells using electron microscopy. Plasma membrane sheets from BHK cells expressing mGFP-wt-H-ras or mGFP-H-rasG12V treated for 24 h with either DMSO control or 0.18 μM CHX were immuno gold-labeled and imaged with an electron microscope. Spatial statistical analysis of the immuno gold point patterns showed that CHX treatment significantly increased nanoclustering not only of constitutively active H-ras but also of full-length wt H-ras (Figure 2a).

We next validated this CHX activity on full-length, constitutively active H-rasG12V using FLIM-FRET. FRET pairs of mGFP- and mCherry fluorescent protein-tagged H-rasG12V were equally expressed in BHK cells that either coexpressed Gal-1, as a positive control of H-rasG12V nanoclustering, or were treated with CHX. At both high and low CHX concentrations, H-ras nanoclustering was significantly enhanced to a comparable level as that with Gal-1 overexpression

DOI: 10.1021/acs.biochem.5b00724
Biochemistry XXXX, XXX, XXX−XXX

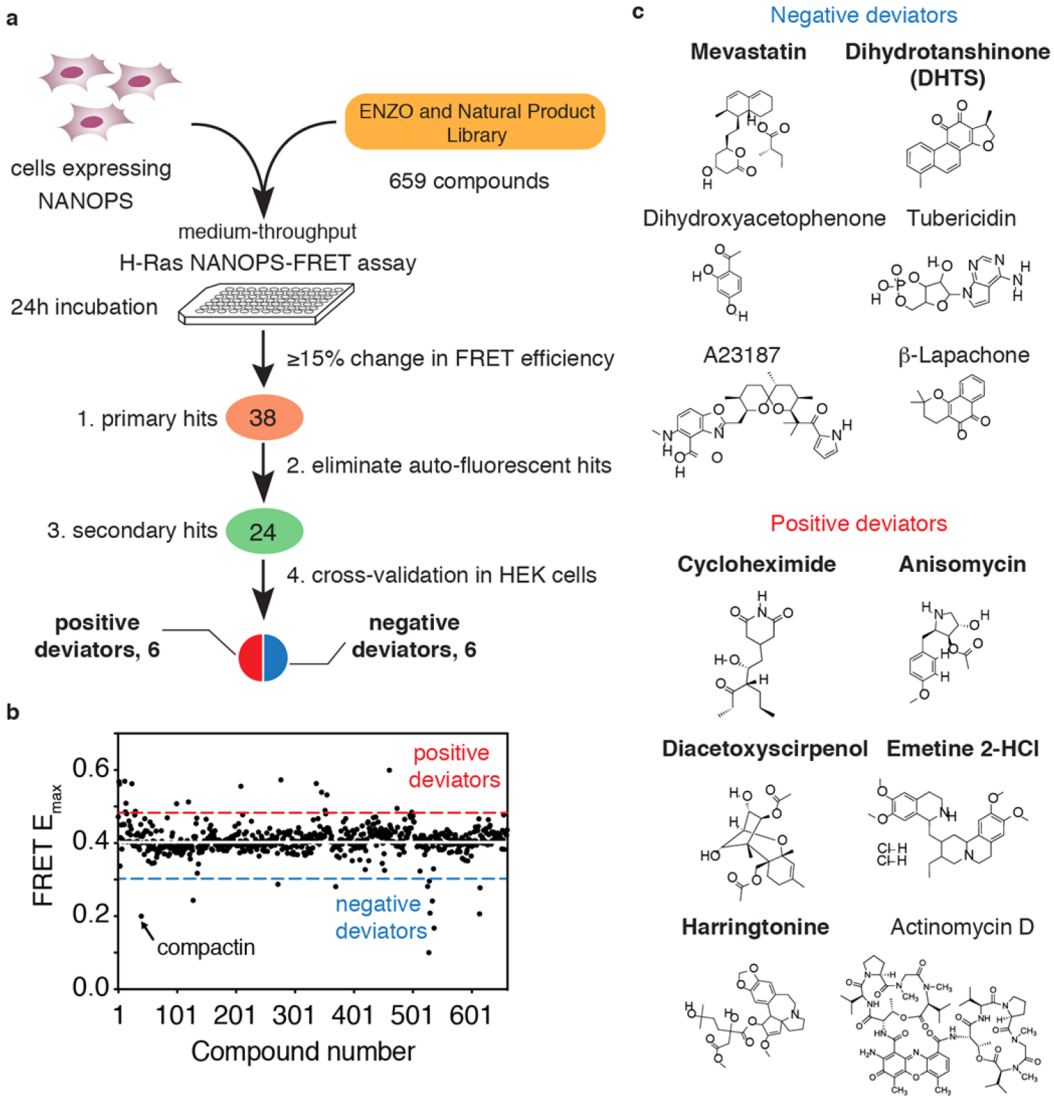

Figure 1. Small molecule chemical screening for specific H-ras modulators. (a) Flowchart of chemical screen with H-ras-NANOPS (NANOcluster and Prenylation Sensors) as a FRET biosensor. (b) Primary screening results. Scatter plot of E_{max} FRET values in BHK cells expressing H-ras-NANOPS treated for 24 h with compounds at 10 μM. Data points represent averages from three independent experiments. White line indicates the average E_{max} of the screened compounds; dotted red and blue lines mark the positive and negative deviator selection threshold of a 15% change from average E_{max}, respectively. (c) Identity and structures of cross-validated hits grouped into negative and positive deviators.

(Figure 2b). Similar results were obtained in HEK cells treated with CHX or two other PSIs (anisomycin and harringtonine) under the same conditions (Supporting Information Figure 3a).

Finally, we completed our assessment of CHX's effect on nanoclustering using a FRAP assay.[17,46] This assay exploits the fact that active H-ras becomes immobilized in nanoclusters.[47] Therefore, the immobile fraction of H-rasG12V measured in FRAP experiments is increased when BHK cells overexpress Gal-1 and decreases when endogenous Gal-1 is depleted (Figure 2c). Consistent with our EM and FRET data, CHX treatment significantly increased the immobile fraction of H-rasG12V to levels comparable to those with Gal-1 overexpression. This panel of state-of-the-art nanocluster experiments firmly establishes CHX as a positive H-ras nanocluster modulator.

Lack of an Effect of Cycloheximide on K-Ras Nanoclustering Supports Isoform Specificity. In order to understand whether these effects of CHX are H-ras isoform-specific, we analyzed the impact of CHX on K-ras, which is organized in laterally segregated nanoclusters distinct from those of H-ras.[15,48]

Spatial analysis of the plasma membrane distribution of K-rasG12V by electron microscopy suggested that CHX does not affect K-rasG12V nanoclustering (Figure 3a). This was confirmed by nanoclustering-FRET of K-rasG12V, which was not affected by CHX, whereas Gal-1 negatively regulated K-ras nanoclustering (Figure 3b). This latter observation can be explained by the phosphatidylserine-mediated negative effect of active H-ras on K-ras nanoclustering,[48] which would be augmented by Gal-1. These data indicate a Gal-1-independent effect of CHX. Altogether, our results establish that CHX specifically increases H-ras nanoclusters but that it has no effect on K-ras nanoclusters.

Our observations that H-ras is specifically affected are in line with those of Ahearn et al., who showed that CHX increases H-ras membrane anchorage and signaling by blocking the prolyl-isomerase FKBP12-stimulated H-ras depalmitoylation.[49] Given the effect of palmitoylation on H-ras nanoscale organization,[50]

DOI: 10.1021/acs.biochem.5b00724
Biochemistry XXXX, XXX, XXX−XXX

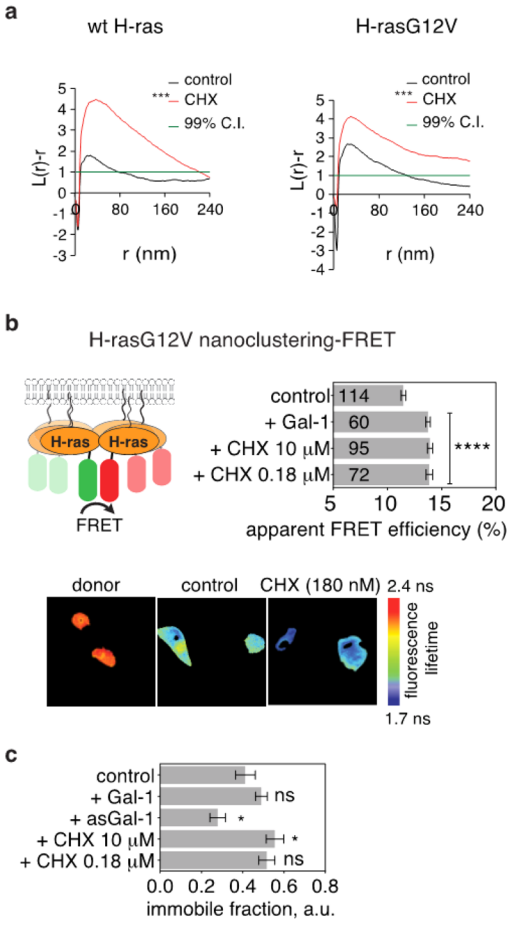

Figure 2. Cycloheximide increases H-ras nanoclustering. (a) Electron microscopic nanoclustering analysis of mGFP-tagged wt H-ras and H-rasG12V in BHK cells in normal medium treated for 24 h with either DMSO control or 0.18 μM CHX. Normalized univariate K-function, where maximal $L(r) - r$ values above the 99% CI for complete spatial randomness indicate clustering at that value of r. Differences between treatment and control were assessed using bootstrap tests (at least 15 images were analyzed for each condition) (***, $p < 0.001$). (b) Top shows a scheme for nanoclustering FRET analysis in BHK cells coexpressing mGFP- and mCherry-tagged H-rasG12V. Cells were treated for 24 h with DMSO control or 0.18 or 10 μM CHX. The apparent FRET efficiency (mean ± SEM, $n = 3$) was calculated from FLIM data. The number in the bars indicates the number of analyzed cells. Bottom shows examples of FLIM-FRET images from the nanoclustering assay as indicated. Image color key on the right shows fluorescence lifetimes. Statistical significance of differences between control and treated cells was examined using one-way ANOVA (****, $p < 0.0001$). (c) Immobile fractions for H-rasG12V measured using FRAP. BHK cells expressing mGFP-H-rasG12V were treated for 24 h with DMSO control or 0.18 or 10 μM CHX or were analyzed after overexpression or antisense (as)-mediated depletion of Gal-1. Statistical significance of differences between control and treated cells was examined using one-way ANOVA (ns, not significant; *, $p < 0.05$).

it is conceivable that the observed retention of palmitoylated H-ras on the plasma membrane under CHX treatment is, in addition, associated with an increase in H-ras nanoclustering.

However, all other protein synthesis inhibitors found in our chemical screen have diverse chemical structures, in line with their different mechanisms of action for protein synthesis inhibition (Supporting Information Table 4). Therefore, inhibition of proteins synthesis, which we demonstrated occurs

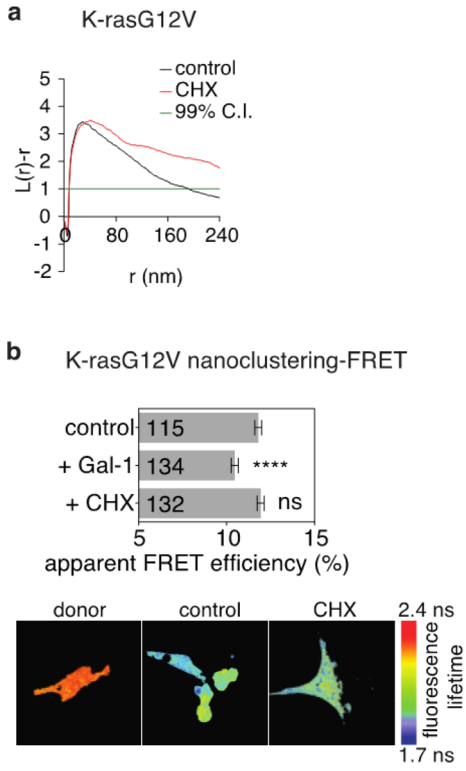

Figure 3. Cycloheximide does not affect K-ras nanoclustering. (a) Electron microscopic nanoclustering analysis of mGFP-tagged K-rasG12V in BHK cells treated for 24 h with either DMSO control or 0.18 μM CHX. Normalized univariate K-function, where maximal $L(r) - r$ values above the 99% CI for complete spatial randomness indicate clustering at that value of r. Differences between treatment and control were assessed using t-tests (ns, not significant). (b) Nanoclustering-FRET analysis in BHK cells coexpressing mGFP- and mCherry-tagged K-rasG12V. Cells were treated for 24 h with either DMSO control or 0.18 μM CHX. The apparent FRET efficiency (mean ± SEM, $n = 3$) was calculated from FLIM data. The number in the bars indicates the number of analyzed cells. Bottom shows examples of FLIM-FRET images from the nanoclustering assay as indicated. Image color key on the right shows fluorescence lifetimes. Statistical significance of differences between control and treated cells was examined using one-way ANOVA (ns, not significant; ****, $p < 0.0001$).

with CHX and with two other PSIs as alternative examples (harringtonine and anisomycin; Supporting Information Figure 2), is the only common denominator among these compounds that all increase H-rasG12V nanoclustering (Figure 1b and Supporting Information Figure 3a). Therefore, our data clearly suggest the existence of an unknown Ras-isoform-specific feedback stemming from protein synthesis to H-ras-nanoclustering.

Cycloheximide Activates H-Ras Effector Recruitment, Downstream Signaling, and PC12 Cell Differentiation. Ras nanoclustering typically correlates with Ras effector recruitment due to the fact that effectors with a high off-rate (such as Raf and PI3K) are recruited only to active Ras in nanoclusters.[17,21] We therefore used our previously established Ras effector recruitment FLIM-FRET assay[17] to analyze the interaction between mGFP-H-rasG12V or mGFP-K-rasG12V and the mRFP-tagged Ras binding domain of C-Raf (RBD) in BHK cells. In line with our nanoclustering data (Figures 2b and 3b), stimulation with CHX significantly increased RBD recruitment to H-rasG12V, whereas the effector recruitment by

DOI: 10.1021/acs.biochem.5b00724
Biochemistry XXXX, XXX, XXX−XXX

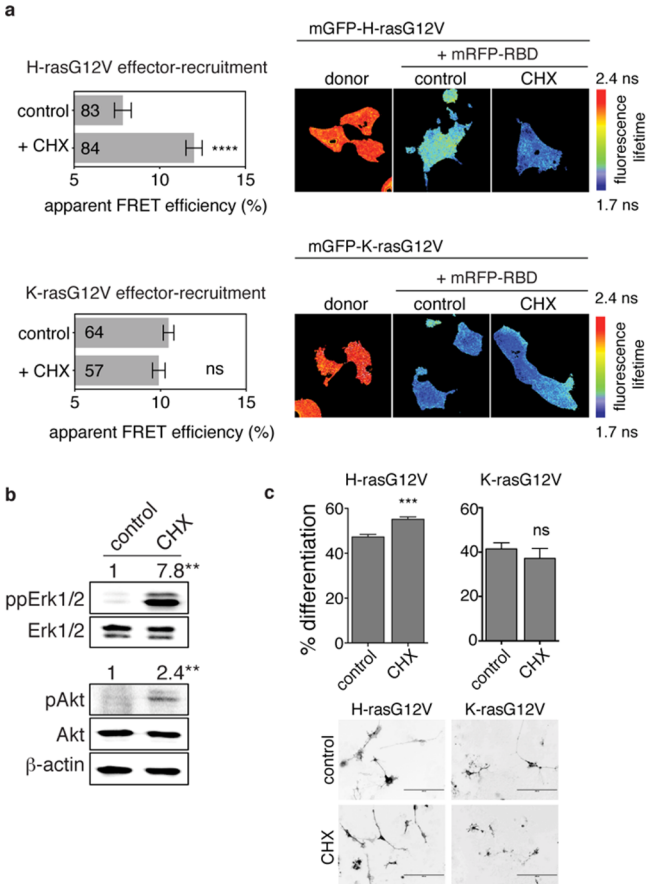

Figure 4. Cycloheximide specifically activates H-ras effector recruitment and Erk and Akt signaling and can drive PC12 cell differentiation. (a) Effector recruitment FRET assay in BHK cells expressing either mGFP-H-rasG12V (top) or mGFP-K-rasG12V (bottom) and mRFP-C-Raf-RBD. Cells were treated for 24 h with either DMSO control or 0.18 μM CHX. The apparent FRET efficiency (mean ± SEM, $n = 3$) was calculated from FLIM data. The number in the bars indicates the number of analyzed cells. On the right are examples of FLIM-FRET images from the effector recruitment assay as indicated. Image color key shows fluorescence lifetimes. Statistical significance of differences between control and treated cells was examined using one-way ANOVA (ns, not significant; ****, $p < 0.0001$). (b) Representative western blots from BHK cells treated for 24 h with 0.18 μM CHX. Numbers indicate the ratio of the phosphorylated Erk and Akt relative to total Erk and Akt, respectively. β-Actin was used as a loading control (mean ± SEM, $n = 3$). Statistical significance was determined using Student's t test (**, $p < 0.01$). (c) PC12 cells transiently transfected with mGFP-H-rasG12V (left) or mGFP-K-rasG12V (right) were incubated with DMSO or 0.18 μM CHX. After 72 h, GFP-positive cells were scored for neurites. Results (top) are plotted as percent of cells (mean ± SEM, $n = 4$) with neurite outgrowth >1.5 times the diameter of the cell body. Representative images of cells (bottom) scored for neurites are shown. Bar represents 200 μm. Statistical significance of differences between control and treated cells was examined using one-way ANOVA (ns, not significant; ***, $p < 0.001$).

K-ras remained unaffected (Figure 4a). These findings suggest that only H-ras signaling is affected by CHX treatment.

Effector recruitment to Ras nanoclusters is the initiating event of its downstream signaling cascades.[17,21] Consequently, we observed that BHK cells treated with CHX displayed significant 7.8- and 2.4-fold increases in Erk1/2 and Akt phosphorylation, respectively (Figure 4b). Similar results were obtained with harringtonine and anisomycin, two other PSI hits (Supporting Information Figure 3b).

Activation of Ras−MAPK is known to induce differentiation of rat adrenal pheochromocytoma (PC12) cells and leads to neurite outgrowth.[51] They are, therefore, a well-established model for MAPK activity and neuronal differentiation independent of growth factor stimulation. Moreover, protein synthesis inhibitors have been previously reported to induce differentiation of neuronal cells.[41] We therefore set out to determine if the increase in H-ras nanoclustering and MAPK signaling by CHX can induce PC12 differentiation. Expression of GFP-H-rasG12V induced differentiation of PC12 cells, as can be seen by neurite formation, and addition of CHX significantly increased the percentage of differentiated cells, but this was not the case with K-rasG12V-expressing cells (Figure 4c). These results demonstrate that protein synthesis inhibitors can augment H-ras nanoclustering and downstream signaling pathways leading to cell differentiation.

CHX Treatment Increases Mammosphere Formation and Tumor Cell Growth *in Ovo*. Both the Erk and Akt signaling pathways are central to cell division and growth and are frequently activated in cancer.[8] In order to confirm that these signaling changes observed here with PSI treatment are H-ras-dependent, we compared ppErk and pAkt levels in MEFs and their H-ras- and N-ras-deficient counterparts (Rasless cells[26]). Indeed, CHX treatment failed to increase ppErk and pAkt levels in Rasless MEFs (Figure 5a, center). Overexpression of wild-type H-ras in Rasless MEFs could restore a significant response to CHX (Figure 5a, right), albeit only partially, due to a low (<20%) transfection efficiency, as established by fluorescence imaging.

We then tested whether the protein synthesis inhibitor CHX would, somewhat paradoxically, be able to drive tumor cell growth in an H-ras-dependent manner. While normal proliferation of MDA-MB-231 breast cancer cells was inhibited by CHX (Supporting Information Figure 4a), growth under nonadherent conditions significantly increased the number of mammospheres (Figure 5b). However, if H-ras was ablated by siRNA, then the number of mammospheres was dramatically reduced (Figure 5c), as would have been expected intuitively from inhibition of protein synthesis. While this effect was less than that by treatment with the CSC drug salinomycin, it was still stronger than that from treatment with the cytotoxic drug doxorubicin and, most importantly, represents a full inversion of the response without H-ras depletion.

We then assessed whether CHX could also affect tumor growth. We used the *in ovo* tumor growth assay as a simple xenograft model. In this assay, human tumor cells grow on the chorioallantoic membrane (CAM) of a chicken embryo. The CAM is a natural immunodeficient host environment capable of sustaining grafted tissues and cells without species-specific restrictions and can be easily adapted to assess the potential effect of drugs on tumor morphology and growth.[52] We grafted human MDA-MB-231 breast cancer cells onto the CAM and treated them with CHX. Consistent with the effect on Ras signaling and mammosphere formation, this treatment led to a significant increase in tumor mass as compared to that of the vehicle-treated control (Figure 5d).

In conclusion, our results suggest that a widely used protein synthesis inhibitor, which is expected to halt cell growth, can drive tumor growth, at least of MDA-MB-231 cells. This effect emerges right at the apex of the Ras−MAPK signaling cascade, specifically at the level of H-ras nanoclustering and effector recruitment.

DOI: 10.1021/acs.biochem.5b00724
Biochemistry XXXX, XXX, XXX−XXX

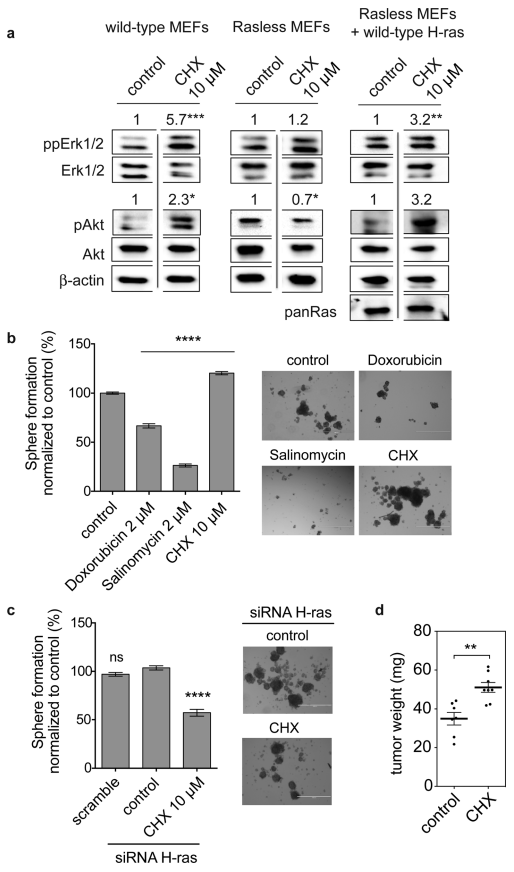

Figure 5. Cycloheximide is an H-ras-dependent tumor growth inducer. (a) Wild-type MEFs (left), Du-315-6 Rasless MEFs (H-ras$^{-/-}$, N-ras$^{-/-}$) (center), and Du-315-6 MEFs transfected with mGFP-wt-H-ras (right) were treated for 24 h with either DMSO control or CHX 10 μM. Numbers indicate the ratio of the phosphorylated Erk and Akt relative to total Erk and Akt, respectively. For H-ras rescue experiments, the obtained ratio was normalized to H-ras overexpression. β-Actin was used as a loading control (mean ± SEM, n = 3; for H-ras rescue, n = 2). Statistical significance was determined using Student's t test (*, $p < 0.05$; **, $p < 0.01$; ***, $p < 0.001$). (b) On the left, the mammosphere forming efficiency of MDA-MB-231 cells grown under nonadherent conditions was measured. Mammospheres were allowed to form for 6 days and were then treated for 3 additional days with either DMSO control or the indicated compounds (mean ± SEM, n = 3). On the right, representative images of mammospheres are shown as indicated. Bar represents 1000 μm. Statistical significance of differences between control and treated cells was examined using one-way ANOVA complemented with Tukey's test (***, $p < 0.001$). (c) Mammosphere forming efficiency was measured with MDA-MB-231 cells transfected with scrambled siRNA or H-ras siRNA and treated with either DMSO control or 10 μM CHX. On the left, the mammosphere forming efficiency was measured as the number of spheres formed and normalized to control (mean ± SEM, n = 4). On the right, representative images of mammospheres are shown as indicated. Bar represents 1000 μm. Statistical significance of differences between control and treated cells was examined using one-way ANOVA complemented with Tukey's test (ns, not significant; ****, $p < 0.0001$). (d) Tumor mass of MDA-MB-231 cells after transplantation onto chick embryo CAM and treatment for 5 days with either DMSO control or 10 μM CHX. The tumor weight was calculated from at least 15 tumors from three independent experiments (mean ± SEM). Statistical significance between control and treated sample was determined using Student's t test (**, $p < 0.01$).

These apparently paradoxical results are somewhat reminiscent of the paradoxical activation of cellular proliferation by Raf inhibitors, which are also known to positively modulate Ras nanoclustering.[45] As in the case of Raf inhibitors, the here described effect of CHX might be relevant only in certain cell types and within a specific expression or genetic context, such as that found in our MDA-MB-231-derived mammospheres. Mammospheres are enriched in cancer stem cells (CSCs), which have different characteristics than the bulk tumor cells, such as increased drug resistance and tumor seeding potential, due to their self-renewal capability.[53]

Little is known about the exact Ras-associated signaling pathways in CSCs. Others[13] and we (A.K. Najumudeen and D. Abankwa, unpublished results) have provided evidence for the divergent roles of Ras isoforms in CSCs. Interestingly, our results here show that CHX increases H-ras signaling output and CSC growth, whereas CHX treatment in combination with H-ras depletion can be synthetically lethal within our CSC model. The synthetic lethality approach proposes the ablation of essential targets in Ras-dependent cancer cells so that it can sensitize these cancer cells to drug treatment.[54] For instance, it has already been shown that depletion of wild-type H- and N-ras in K-ras mutant cancer cells can sensitize these cancer cells to DNA damaging agents.[55] Our data indicate the significance of PSIs and similar compounds, such as proteasome inhibitors, as (antagonistic) tool compounds for studying synthetic lethalities.

Ras signaling converges both via the PI3K–Akt–mTORC1 and Raf–Erk–RSK pathways on protein translation through the regulation of the activities of S6K and eIF4E.[56,57] The kind of feedback from protein synthesis toward H-ras that is being engaged is currently unknown. It is well-known that plasma membrane lipids such as cholesterol and phosphatidylserine play an important role in the proper lateral segregation of Ras isoforms into distinct nanoclusters.[48] Considering that lipid metabolism is regulated by mTORC1,[58] changes in protein synthesis rate, such as that induced by PSI treatment, may conversely alter the lipid profile in the plasma membrane and thus affect Ras nanoclustering.

Importantly, our results strongly suggest that PSIs in combination with H-ras depletion can act synthetically lethal within CSCs. In agreement with a number of recent reports, our findings suggest new drug targeting opportunities at the nexus between protein synthesis and Ras–MAPK signaling in cancer.[59,60]

■ ASSOCIATED CONTENT

Supporting Information

The Supporting Information is available free of charge on the ACS Publications website at DOI: 10.1021/acs.biochem.5b00724.

Additional experimental procedures; cross-validation of hits in HEK293-EBNA cells; PSI treatment inhibits protein translation; PSIs increase H-ras nanoclustering and Erk–Akt signaling; CHX inhibits normal proliferation of MDA-MB-231; list of compounds; list of primary hits from the ENZO and NP library screens with H-ras-NANOPS using cytometry-FRET; list of cross-validated hits in BHK and HEK cells; list of validated protein synthesis inhibitor activities (PDF)

■ AUTHOR INFORMATION

Corresponding Author

*E-mail: daniel.abankwa@btk.fi.

DOI: 10.1021/acs.biochem.5b00724
Biochemistry XXXX, XXX, XXX–XXX

Author Contributions

D.A. conceived the project. A.K.N. acquired and analyzed the screening and FRET data and performed PC12 and proliferation experiments. I.M.D.P. acquired and analyzed the FRET data and performed western blot, β-galactosidase, PC12, and mammosphere experiments. B.L. performed western blot and mammosphere experiments. Y.Z. and J.H. designed and performed the EM experiments. S.K.-J.L. acquired and analyzed the CAM tumor data. A.F. and P.V. optimized and managed the chemical libraries. A.K.N, I.M.D.P., and D.A. designed the experiments and wrote the manuscript.

Funding

This work was supported by an Academy of Finland fellowship grant, the Sigrid Juselius Foundation, the Cancer Society of Finland, a Marie-Curie Reintegration Grant, and Jane and Aatos Erkko Foundation grants to D.A. and by a Texas Digestive Diseases Center Pilot and Feasibility grant (P30 DK56338) to Y.Z. and CPRIT (Cancer Prevention Research Institute of Texas) grant (RP130059) to J.H. A.K.N. was supported by the ISB graduate school. A.F and P.V. acknowledge the financial support of the Drug Discovery and Chemical Biology (DDCB) network of Biocenter Finland and the NordForsk Nordic Chemical Biology network (to Pharmaceutical Biology Research Group). S.K.-J.L. was supported by The Swedish Cultural Foundation of Finland, Magnus Ehrnrooth Foundation, Waldemar von Frenckell Foundation, K. Albin Johansson Foundation, and Knut and Alice Wallenberg Foundation.

Notes

The authors declare no competing financial interest.

■ ACKNOWLEDGMENTS

We thank Christina-Oetken Lindholm for experimental support, Maja Šolman and Camilo Guzmán for support with FRAP data analysis, and Yonatan Gebremariam Mideksa for help with ChemDraw. siRNA directed against H-ras was provided as a kind gift from Prof. Jukka Westermarck's group.[31]

■ REFERENCES

(1) Arteaga, C. L., and Engelman, J. A. (2014) ERBB receptors: from oncogene discovery to basic science to mechanism-based cancer therapeutics. *Cancer Cell 25*, 282−303.

(2) Pemovska, T., Kontro, M., Yadav, B., Edgren, H., Eldfors, S., Szwajda, A., Almusa, H., Bespalov, M. M., Ellonen, P., Elonen, E., Gjertsen, B. T., Karjalainen, R., Kulesskiy, E., Lagström, S., Lehto, A., Lepistö, M., Lundán, T., Majumder, M. M., Marti, J. M. L., Mattila, P., Murumägi, A., Mustjoki, S., Palva, A., Parsons, A., Pirttinen, T., Rämet, M. E., Suvela, M., Turunen, L., Västrik, I., Wolf, M., Knowles, J., Aittokallio, T., Heckman, C. A., Porkka, K., Kallioniemi, O., and Wennerberg, K. (2013) Individualized systems medicine strategy to tailor treatments for patients with chemorefractory acute myeloid leukemia. *Cancer Discovery 3*, 1416−1429.

(3) Ebben, J. D., Treisman, D. M., Zorniak, M., Kutty, R. G., Clark, P. A., and Kuo, J. S. (2010) The cancer stem cell paradigm: a new understanding of tumor development and treatment. *Expert Opin. Ther. Targets 14*, 621−632.

(4) Davies, S. G., Kennewell, P. D., Russell, A. J., Seden, P. T., Westwood, R., and Wynne, G. M. (2015) Stemistry: The Control of Stem Cells in Situ Using Chemistry. *J. Med. Chem. 58*, 2863−2894.

(5) Pao, W., Miller, V. A., Politi, K. A., Riely, G. J., Somwar, R., Zakowski, M. F., Kris, M. G., and Varmus, H. (2005) Acquired resistance of lung adenocarcinomas to gefitinib or erlotinib is associated with a second mutation in the EGFR kinase domain. *PLoS Med. 2*, e73.

(6) Groenendijk, F. H., and Bernards, R. (2014) Drug resistance to targeted therapies: Déjà vu all over again. *Mol. Oncol. 8*, 1067−1083.

(7) Ledford, H. (2015) Cancer: The Ras renaissance. *Nature 520*, 278−280.

(8) Steelman, L. S., Chappell, W. H., Abrams, S. L., Kempf, R. C., Long, J., Laidler, P., Mijatovic, S., Maksimovic-Ivanic, D., Stivala, F., Mazzarino, M. C., Donia, M., Fagone, P., Malaponte, G., Nicoletti, F., Libra, M., Milella, M., Tafuri, A., Bonati, A., Bäsecke, J., Cocco, L., Evangelisti, C., Martelli, A. M., Montalto, G., Cervello, M., and McCubrey, J. A. (2011) Roles of the Raf/MEK/ERK and PI3K/PTEN/Akt/mTOR pathways in controlling growth and sensitivity to therapy-implications for cancer and aging. *Aging (Albany NY) 3*, 192−222.

(9) Elad-Sfadia, G., Haklai, R., Ballan, E., Gabius, H.-J., and Kloog, Y. (2002) Galectin-1 augments Ras activation and diverts Ras signals to Raf-1 at the expense of phosphoinositide 3-kinase. *J. Biol. Chem. 277*, 37169−37175.

(10) Prior, I. A., Lewis, P. D., and Mattos, C. (2012) A comprehensive survey of Ras mutations in cancer. *Cancer Res. 72*, 2457−2467.

(11) Umanoff, H., Edelmann, W., Pellicer, A., and Kucherlapati, R. (1995) The murine N-ras gene is not essential for growth and development. *Proc. Natl. Acad. Sci. U. S. A. 92*, 1709−1713.

(12) Johnson, L., Greenbaum, D., Cichowski, K., Mercer, K., Murphy, E., Schmitt, E., Bronson, R. T., Umanoff, H., Edelmann, W., Kucherlapati, R., and Jacks, T. (1997) K-ras is an essential gene in the mouse with partial functional overlap with N-ras. *Genes Dev. 11*, 2468−2481.

(13) Quinlan, M. P., Quatela, S. E., Philips, M. R., and Settleman, J. (2008) Activated Kras, but Not Hras or Nras, May Initiate Tumors of Endodermal Origin via Stem Cell Expansion. *Molecular and cellular biology 28*, 2659−2674.

(14) Fernandez-Medarde, A., and Santos, E. (2011) Ras in Cancer and Developmental Diseases. *Genes Cancer 2*, 344−358.

(15) Plowman, S. J., Muncke, C., Parton, R. G., and Hancock, J. F. (2005) H-ras, K-ras, and inner plasma membrane raft proteins operate in nanoclusters with differential dependence on the actin cytoskeleton. *Proc. Natl. Acad. Sci. U. S. A. 102*, 15500−15505.

(16) Prior, I. A., Muncke, C., Parton, R. G., and Hancock, J. F. (2003) Direct visualization of Ras proteins in spatially distinct cell surface microdomains. *J. Cell Biol. 160*, 165−170.

(17) Guzmán, C., Solman, M., Ligabue, A., Blazevitš, O., Andrade, D. M., Reymond, L., Eggeling, C., and Abankwa, D. (2014) The efficacy of Raf kinase recruitment to the GTPase H-ras depends on H-ras membrane conformer-specific nanoclustering. *J. Biol. Chem. 289*, 9519−9533.

(18) Abankwa, D., Gorfe, A. A., and Hancock, J. F. (2007) Ras nanoclusters: molecular structure and assembly. *Semin. Cell Dev. Biol. 18*, 599−607.

(19) Zhou, Y., and Hancock, J. F. (2015) Ras nanoclusters: Versatile lipid-based signaling platforms. *Biochim. Biophys. Acta, Mol. Cell Res. 1853*, 841−849.

(20) Belanis, L., Plowman, S. J., Rotblat, B., Hancock, J. F., and Kloog, Y. (2008) Galectin-1 is a novel structural component and a major regulator of h-ras nanoclusters. *Mol. Biol. Cell 19*, 1404−1414.

(21) Tian, T., Harding, A., Inder, K., Plowman, S., Parton, R. G., and Hancock, J. F. (2007) Plasma membrane nanoswitches generate high-fidelity Ras signal transduction. *Nat. Cell Biol. 9*, 905−914.

(22) Köhnke, M., Schmitt, S., Ariotti, N., Piggott, A. M., Parton, R. G., Lacey, E., Capon, R. J., Alexandrov, K., and Abankwa, D. (2012) Design and Application of In Vivo FRET Biosensors to Identify Protein Prenylation and Nanoclustering Inhibitors. *Chem. Biol. 19*, 866−874.

(23) Najumudeen, A. K., Köhnke, M., Solman, M., Alexandrov, K., and Abankwa, D. (2013) Cellular FRET-Biosensors to Detect Membrane Targeting Inhibitors of N-Myristoylated Proteins. *PLoS One 8*, e66425.

(24) Najumudeen, A. K., Guzmán, C., Posada, I. M. D., and Abankwa, D. (2015) Rab-NANOPS: FRET biosensors for Rab membrane nanoclustering and prenylation detection in mammalian cells. *Methods Mol. Biol. 1298*, 29−45.

DOI: 10.1021/acs.biochem.5b00724
Biochemistry XXXX, XXX, XXX−XXX

(25) Coxon, F., Joachimiak, Ł., Najumudeen, A. K., Breen, G., Gmach, J., Oetken-Lindholm, C., Way, R., Dunford, J., Abankwa, D., and Błażewska, K. M. (2014) Synthesis and characterization of novel phosphonocarboxylate inhibitors of RGGT. *Eur. J. Med. Chem. 84*, 77−89.
(26) Drosten, M., Drosten, M., Dhawahir, A., Dhawahir, A., Sum, E. Y. M., Sum, E. Y. M., Urosevic, J., Urosevic, J., Lechuga, C. G., Lechuga, C. G., Esteban, L. M., Esteban, L. M., Castellano, E., Castellano, E., Guerra, C., Guerra, C., Santos, E., Santos, E., Barbacid, M., and Barbacid, M. (2010) Genetic analysis of Ras signalling pathways in cell proliferation, migration and survival. *EMBO J. 29*, 1091−1104.
(27) Meissner, P., Pick, H., Kulangara, A., Chatellard, P., Friedrich, K., and Wurm, F. M. (2001) Transient gene expression: recombinant protein production with suspension-adapted HEK293-EBNA cells. *Biotechnol. Bioeng. 75*, 197−203.
(28) Abankwa, D., Hanzal-Bayer, M., Ariotti, N., Plowman, S. J., Gorfe, A. A., Parton, R. G., McCammon, J. A., and Hancock, J. F. (2008) A novel switch region regulates H-ras membrane orientation and signal output. *EMBO J. 27*, 727−735.
(29) Abankwa, D., Gorfe, A. A., Inder, K., and Hancock, J. F. (2010) Ras membrane orientation and nanodomain localization generate isoform diversity. *Proc. Natl. Acad. Sci. U. S. A. 107*, 1130−1135.
(30) Paz, A., Haklai, R., Elad-Sfadia, G., Ballan, E., and Kloog, Y. (2001) Galectin-1 binds oncogenic H-Ras to mediate Ras membrane anchorage and cell transformation. *Oncogene 20*, 7486−7493.
(31) Kauko, O., Laajala, T. D., Jumppanen, M., Hintsanen, P., Suni, V., Haapaniemi, P., Corthals, G., Aittokallio, T., Westermarck, J., and Imanishi, S. Y. (2015) Label-free quantitative phosphoproteomics with novel pairwise abundance normalization reveals synergistic RAS and CIP2A signaling. *Sci. Rep. 5*, 13099.
(32) Brunhofer, G., Fallarero, A., Karlsson, D., Batista-Gonzalez, A., Shinde, P., Gopi Mohan, C., and Vuorela, P. (2012) Exploration of natural compounds as sources of new bifunctional scaffolds targeting cholinesterases and beta amyloid aggregation: The case of chelerythrine. *Bioorg. Med. Chem. 20*, 6669−6679.
(33) Narwal, M., Fallarero, A., Vuorela, P., and Lehtiö, L. (2012) Homogeneous screening assay for human tankyrase. *J. Biomol. Screening 17*, 593−604.
(34) Abankwa, D., and Vogel, H. (2007) A FRET map of membrane anchors suggests distinct microdomains of heterotrimeric G proteins. *J. Cell Sci. 120*, 2953−2962.
(35) Prior, I. A., Parton, R. G., and Hancock, J. F. (2003) Observing cell surface signaling domains using electron microscopy. *Sci. Signaling 2003*, PL9.
(36) Feder, T. J., Brust-Mascher, I., Slattery, J. P., Baird, B., and Webb, W. W. (1996) Constrained diffusion or immobile fraction on cell surfaces: a new interpretation. *Biophys. J. 70*, 2767−2773.
(37) Brown, M. S., Faust, J. R., Goldstein, J. L., Kaneko, I., and Endo, A. (1978) Induction of 3-hydroxy-3-methylglutaryl coenzyme A reductase activity in human fibroblasts incubated with compactin (ML-236B), a competitive inhibitor of the reductase. *J. Biol. Chem. 253*, 1121−1128.
(38) Lee, D. S., Lee, S. H., Ha, S. C., Seu, Y. B., and Hong, S. D. (1998) Dihydrotanshinone I is an inhibitor of farnesyl-protein transferase. *Kor J. Life Sci. 8*, 158−161.
(39) Greenberg, M. E., Hermanowski, A. L., and Ziff, E. B. (1986) Effect of protein synthesis inhibitors on growth factor activation of c-fos, c-myc, and actin gene transcription. *Mol. Cell. Biol. 6*, 1050−1057.
(40) Grollman, A. P. (1967) Inhibitors of protein biosynthesis. II. Mode of action of anisomycin. *J. Biol. Chem. 242*, 3226−3233.
(41) Louis, J. C., Burnham, P., and Varon, S. (1994) Neurite outgrowth from cultured CNS neurons is promoted by inhibitors of protein and RNA synthesis. *J. Neurobiol. 25*, 209−217.
(42) Rotblat, B., Belanis, L., Liang, H., Haklai, R., Elad-Zefadia, G., Hancock, J. F., Kloog, Y., and Plowman, S. J. (2010) H-Ras nanocluster stability regulates the magnitude of MAPK signal output. *PLoS One 5*, e11991.
(43) Zaret, K. S. (2009) Using Small Molecules to Great Effect in Stem Cell Differentiation. *Stem Cell 4*, 373−374.
(44) Hatzivassiliou, G., Song, K., Yen, I., Brandhuber, B. J., Anderson, D. J., Alvarado, R., Ludlam, M. J. C., Stokoe, D., Gloor, S. L., Vigers, G., Morales, T., Aliagas, I., Liu, B., Sideris, S., Hoeflich, K. P., Jaiswal, B. S., Seshagiri, S., Koeppen, H., Belvin, M., Friedman, L. S., and Malek, S. (2010) RAF inhibitors prime wild-type RAF to activate the MAPK pathway and enhance growth. *Nature 464*, 431−435.
(45) Cho, K.-J., Kasai, R. S., Park, J.-H., Chigurupati, S., Heidorn, S. J., van der Hoeven, D., Plowman, S. J., Kusumi, A., Marais, R., and Hancock, J. F. (2012) Raf inhibitors target ras spatiotemporal dynamics. *Curr. Biol. 22*, 945−955.
(46) Guzmán, C., Solman, M., and Abankwa, D. (2014) Nano-clustering and heterogeneous membrane diffusion of Ras studied by FRAP and RICS analysis. *Methods Mol. Biol. 1120*, 307−326.
(47) Hancock, J. F., and Parton, R. G. (2005) Ras plasma membrane signalling platforms. *Biochem. J. 389*, 1−11.
(48) Zhou, Y., Liang, H., Rodkey, T., Ariotti, N., Parton, R. G., and Hancock, J. F. (2014) Signal Integration by Lipid-Mediated Spatial Cross Talk between Ras Nanoclusters. *Molecular and cellular biology 34*, 862−876.
(49) Ahearn, I. M., Tsai, F. D., Court, H., Zhou, M., Jennings, B. C., Ahmed, M., Fehrenbacher, N., Linder, M. E., and Philips, M. R. (2011) FKBP12 binds to acylated H-ras and promotes depalmitoylation. *Mol. Cell 41*, 173−185.
(50) Roy, S., Plowman, S., Rotblat, B., Prior, I. A., Muncke, C., Grainger, S., Parton, R. G., Henis, Y. I., Kloog, Y., and Hancock, J. F. (2005) Individual palmitoyl residues serve distinct roles in H-ras trafficking, microlocalization, and signaling. *Molecular and cellular biology 25*, 6722−6733.
(51) Bar-Sagi, D., and Feramisco, J. R. (1985) Microinjection of the ras oncogene protein into PC12 cells induces morphological differentiation. *Cell 42*, 841−848.
(52) Lokman, N. A., Elder, A. S. F., Ricciardelli, C., and Oehler, M. K. (2012) Chick Chorioallantoic Membrane (CAM) Assay as an In Vivo Model to Study the Effect of Newly Identified Molecules on Ovarian Cancer Invasion and Metastasis. *Int. J. Mol. Sci. 13*, 9959−9970.
(53) Kreso, A., and Dick, J. E. (2014) Evolution of the Cancer Stem Cell Model. *Cell Stem Cell 14*, 275−291.
(54) Downward, J. (2015) RAS Synthetic Lethal Screens Revisited: Still Seeking the Elusive Prize? *Clin. Cancer Res. 21*, 1802−1809.
(55) Grabocka, E., Pylayeva-Gupta, Y., Jones, M. J. K., Lubkov, V., Yemanaberhan, E., Taylor, L., Jeng, H. H., and Bar-Sagi, D. (2014) Wild-type H- and N-Ras promote mutant K-Ras-driven tumorigenesis by modulating the DNA damage response. *Cancer Cell 25*, 243−256.
(56) Carracedo, A., and Pandolfi, P. P. (2008) The PTEN-PI3K pathway: of feedbacks and cross-talks. *Oncogene 27*, 5527−5541.
(57) Laplante, M., and Sabatini, D. M. (2012) mTOR Signaling in Growth Control and Disease. *Cell 149*, 274−293.
(58) Ricoult, S. J. H., and Manning, B. D. (2012) The multifaceted role of mTORC1 in the control of lipid metabolism. *EMBO Rep. 14*, 242−251.
(59) Leprivier, G., Remke, M., Rotblat, B., Dubuc, A., Mateo, A.-R. F., Kool, M., Agnihotri, S., El-Naggar, A., Yu, B., Somasekharan, S. P., Faubert, B., Bridon, G., Tognon, C. E., Mathers, J., Thomas, R., Li, A., Barokas, A., Kwok, B., Bowden, M., Smith, S., Wu, X., Korshunov, A., Hielscher, T., Northcott, P. A., Galpin, J. D., Ahern, C. A., Wang, Y., McCabe, M. G., Collins, V. P., Jones, R. G., Pollak, M., Delattre, O., Gleave, M. E., Jan, E., Pfister, S. M., Proud, C. G., Derry, W. B., Taylor, M. D., and Sorensen, P. H. (2013) The eEF2 Kinase Confers Resistance to Nutrient Deprivation byBlocking Translation Elongation. *Cell 153*, 1064−1079.
(60) Boussemart, L., Malka-Mahieu, H., Girault, I., Allard, D., Hemmingsson, O., Tomasic, G., Thomas, M., Basmadjian, C., Ribeiro, N., Thuaud, F., Mateus, C., Routier, E., Kamsu-Kom, N., Agoussi, S., Eggermont, A. M., Désaubry, L., Robert, C., and Vagner, S. (2014) eIF4F is a nexus of resistance to anti-BRAF and anti-MEK cancer therapies. *Nature 513*, 105−109.

DOI: 10.1021/acs.biochem.5b00724
Biochemistry XXXX, XXX, XXX−XXX